Research Square

Preprints are preliminary reports that have not undergone peer review.
They should not be considered conclusive, used to inform clinical practice,
or referenced by the media as validated information.

Dissociation of Skin Tau-Seeding Activity from Classical Plasma Alzheimer's Biomarkers in Parkinson's Disease

Yijia Chen
First Affiliated Hospital of Nanchang University
Yuhe Wu
First Affiliated Hospital of Nanchang University
Kuan Ning
First Affiliated Hospital of Nanchang University
Zerui Wang
Guangzhou Medical University
Zhihong Jie
First Affiliated Hospital of Nanchang University
Hengxu Mao
Guangzhou Medical University
Yaojun Kuang
Guangzhou Medical University
Hancun Yi
First Affiliated Hospital of Nanchang University
Alessandro Furia
University of Bologna
Zihao Zhang
First Affiliated Hospital of Nanchang University
Yuejun Gu
First Affiliated Hospital of Nanchang University
Mengting Ting
First Affiliated Hospital of Nanchang University
Yuyang Shi
First Affiliated Hospital of Nanchang University
Jianfeng Huang
First Affiliated Hospital of Nanchang University
Yifan Wang
First Affiliated Hospital of Nanchang University
Xinjian Fan

First Affiliated Hospital of Nanchang University

Shiyang Li
First Affiliated Hospital of Nanchang University

Xianwei Cao
First Affiliated Hospital of Nanchang University

Pingping Shen
Jilin University

Xia Huang
First Affiliated Hospital of Nanchang University

Vincenzo Donadio
University of Bologna

Chengsi Wu
First Affiliated Hospital of Nanchang University

Jie Zhang
First Affiliated Hospital of Nanchang University

Ping-Yi Xu
Guangzhou Medical University

Xin Fang
First Affiliated Hospital of Nanchang University

Daojun Hong
First Affiliated Hospital of Nanchang University

Wenquan Zou
wenquanzou@ncu.edu.cn

First Affiliated Hospital of Nanchang University

Article

Keywords: Parkinson's disease, α-synuclein (αSyn), skin, biomarker, Real-time quaking-induced conversion (RT-QuIC) assay, synucleinopathies, multiple system atrophy (MSA), dementia with Lewy bodies (DLB), Alzheimer's disease, phosphorylated tau 217 (p-tau217)

Posted Date: August 10th, 2026

DOI: https://doi.org/10.21203/rs.3.rs-10552678/v1

License: This work is licensed under a Creative Commons Attribution 4.0 International License. Read Full License

Additional Declarations: No competing interests reported.

Abstract

Parkinson's disease (PD) is neuropathologically defined by α-synuclein (αSyn) aggregation, yet nearly half of patients exhibit comorbid tau-pathology indicated by neuropathological examination. Using skin RT-QuIC and plasma biomarkers [p-tau217, glial fibrillary acidic protein (GFAP), neurofilament light chain (NfL)], we assessed αSyn- and tau-seeding across independent PD cohorts. αSyn-seeding demonstrated robust diagnostic performance, discriminating PD from controls with ~ 90–95% sensitivity and specificity. Surprisingly, 40–50% of PD patients showed positive skin tau-seeding; however, all PD subgroups, regardless of tau status, displayed plasma p-tau217 and GFAP levels indistinguishable from controls, starkly contrasting with Alzheimer's disease (AD) where marked elevations occurred. Skin tau correlated with plasma p-tau217 in AD, but not in PD, and tau fibrils from PD were morphologically distinct from AD. Thus, skin tau-seeding in PD may reflect a non-AD tauopathy independent of classical biomarkers, challenging diagnostic assumptions and underscoring the need for multimodal strategies to guide personalized stratification.

Introduction

Parkinson’s disease (PD) is the second most common neurodegenerative disorder, characterized by the accumulation of misfolded α-synuclein (αSyn) in Lewy bodies and neurites and the loss of dopaminergic neurons in the brain. However, the clinical and pathological heterogeneity of PD is increasingly recognized, with comorbid pathologies significantly influencing disease progression, cognitive decline, and therapeutic responses[1–4]. Among these, tau pathology is frequently observed in PD patients at autopsy, often correlating with a more aggressive cognitive trajectory[5–7].

The advent of fluid biomarkers has revolutionized the *in vivo* detection of the Alzheimer’s disease (AD) pathology. Specifically, plasma phosphorylated tau at threonine 217 (p-tau217) has demonstrated exceptional specificity and sensitivity for identifying cortical β-amyloid and tau pathology, distinguishing AD from other neurodegenerative disorders with high accuracy[8,9]. Consequently, elevated plasma p-tau217 is now considered a reliable proxy for ongoing AD-type neurodegeneration.

The advent of seed amplification assays (SAAs), notably real-time quaking-induced conversion (RT-QuIC), has enabled the ultrasensitive detection of misfolded protein seeds in peripheral tissues. Skin biopsy has emerged as a particularly promising, minimally invasive approach for detecting αSyn seeds in patients with PD and other synucleinopathies[10–16]. Extending this methodology, tau RT-QuIC assays have recently been applied to skin samples, demonstrating successful detection of tau-seeding activity in patients with Alzheimer's disease (AD) and tauopathy[17–19], and, notably, in synucleinopathy patients as well, though at intermediate levels between healthy controls and AD patients[17]. However, the clinical significance of skin tau-seeding activity in PD, and whether it correlates with systemic AD biomarker profiles (as reflected by plasma p-tau217), remain to be established.

Here, we address this gap by simultaneously evaluating skin αSyn- and tau-seeding activities in two PD cohorts using optimized RT-QuIC assays. We further integrate these findings with ultrasensitive single molecular array (Simoa)-detected AD-related plasma biomarkers including p-tau217, glial fibrillary acidic protein (GFAP) and neurofilament light chain (NfL) to determine whether skin tau positivity in PD reflects the classical AD-related peripheral signature in a comorbid condition. Our results reveal not only high sensitivity and specificity of the skin αSyn- and tau-seeding activity for distinguishing PD and AD from controls but also a surprising dissociation: a substantial subset of PD patients exhibits positive skin tau-seeding activity while maintaining plasma p-tau217 levels indistinguishable from healthy controls, suggesting the existence of a distinct, non-AD tauopathy in PD patients.

Results

RT-QuIC titration of human αSyn pre-formed fibrils and end-product characterization of their de novo aggregates

After the monomeric and pre-formed fibrils (PFFs) of the recombinant human and mouse αSyn were prepared from *E*. coli, purified with FPLC, and confirmed by Coomassie blue staining, western blotting, far-UV CD, Congo red staining and TEM (Supplementary Fig. S1, S2), we first characterized the assay sensitivity using recombinant human αSyn PFFs as the seeds while the mouse monomeric αSyn served as the substrate and control seeds. Real-time kinetic ThT fluorescence assays performed using serial dilutions of αSyn PFFs from 10^{-2} to 10^{-6} revealed a significant increase in fluorescence within approximately 10 hours for the PFF-seeded reactions, whereas monomer-seeded controls remained largely inactive until ~ 35 hours for the 10^{-2} dilution (Fig. 1a). The seeding activity of human αSyn PFFs exhibited a clear dose-dependent relationship, influencing both the maximum ThT intensity and the duration of the lag phase. In contrast, reactions containing the αSyn monomer seeds showed a fluorescence increase only after ~ 35 hours, which occurred independently of concentration, a characteristic of non-specific aggregation. The maximal dilution that reliably discriminated PFFs from monomer was 10^{-5}, corresponding to a seeding concentration of approximately 0.14 fg/mL.

Biochemical and morphological analyses of the RT-QuIC end-products confirmed the specificity of the reaction. Fluorescence microscopy (FM) and Congo red staining (CRS) revealed strong fluorescence intensity and reddish-stained structures exclusively in PFF-seeded reactions (Fig. 1c, e), which were absent in monomer control-seeded end products (Fig. 1b, d). TEM further confirmed the abundant presence of typical amyloid fibrils in PFF-seeded products (Fig. 1g), contrasting with the empty fields seen in monomer controls (Fig. 1f).

Clinical validation of αSyn RT-QuIC in skin biopsies from PD patients

Following optimization, we applied the αSyn RT-QuIC assay to skin biopsies obtained from retrospective cohorts of patients with retrospective PD (rPD, n = 43), multiple system atrophy (MSA, n = 21), dementia

with Lewy bodies (DLB, n = 3), and normal controls (CTL, n = 34) (Table 1). Clinical diagnoses were confirmed using established criteria and corroborated by DAT-PET and FDG-PET imaging (Table 1). Kinetic curves exhibited distinct, rapid amplification profiles for all disease groups compared with CTL (Fig. 2a). Endpoint ThT fluorescence intensities were significantly elevated across all disease groups relative to CTL, with rPD and MSA samples producing particularly robust signals (Fig. 2b). ROC analysis demonstrated strong diagnostic accuracy, effectively differentiating rPD from CTL (AUC = 0.972; sensitivity, 90.7%; specificity, 94.12%; Fig. 2c and Table 2) and MSA from CTL (AUC = 0.993; sensitivity, 100%; specificity, 94.12%; Fig. 2d and Table 2). To further validate these findings, we assessed diagnostic performance using alternative thresholding approaches, specifically, defining cutoffs based on the mean plus standard deviations (SD) of control values and on well-count criteria. Notably, both methods yielded sensitivity and specificity estimates closely matching those derived from ROC analysis (Table 2).

Following the derivation of diagnostic criteria from well-count and fluorescence cutoff thresholds for αSyn-seeding positivity, we proceeded to validate the assay using an independent prospective cohort of 104 patients with possible PD (pPD). Replicating our retrospective observations, endpoint ThT fluorescence was markedly elevated in pPD compared to CTL (Fig. 2b), translating to a sensitivity of 91.3% for the well-count-based and a sensitivity of 90.4% for the cutoff-based criteria (Table 2), based on the criteria established from the retrospective PD cohort above. ROC analysis of the pPD cohort yielded an AUC of 0.96 (Fig. 2e). Together, these three independent lines of evidence including well-count positivity, fluorescence cutoffs, and ROC performance in both retrospective and prospective PD cohorts affirm the clinical utility of this skin-based approach, which employed recombinant mouse αSyn as the substrate in the refined RT-QuIC assay.

Characterization of αSyn aggregates in patient-derived end-products

To verify that the ThT signal reflected authentic αSyn aggregation, we characterized end-products from rPD and control reactions using the following sophisticated approaches. FTA is a method that can trapped the detergent-insoluble large protein aggregates through a filter membrane and detected the trapped aggregates by immunoreacting with a specific antibody[20,21]. The blots probed with anti-αSyn antibody D37A6 showed robust immunoreactive bands in rPD-seeded samples, whereas CTL-seeded products exhibited only negligible background staining (Fig. 3a, b). The FTA band intensity showed a moderate positive correlation with endpoint ThT fluorescence intensity (Fig. 3c). FM and CRS confirmed the presence of fluorescent and Congo red-positive amyloid deposits exclusively in rPD samples (Fig. 3e, g), with controls showing no such structures (Fig. 3d, f). Critically, TEM imaging verified the presence of abundant, morphologically typical amyloid fibrils in rPD-seeded reactions (Fig. 3i), whereas no filamentous material was detected in CTL-derived end-products (Fig. 3h). Similar confirmatory results were obtained in samples from MSA and DLB patients (Supplementary Fig. S3), validating the assay across the spectrum of synucleinopathies.

Detection and differentiation of tau-seeding activity in skin of patients with PD or other conditions

Recognizing that co-pathologies often complicate clinical diagnoses, we employed the RT-QuIC platform to detect tau-seeding activity in the same skin extracts from PD and other conditions. As reported previously, AD skin samples exhibited markedly higher tau-seeding compared to CTL (46.57% ± 18.8% vs 4.2% ± 1.6%, $p < 0.0001$) and all synucleinopathy groups [rPD (14.4% ± 7.4%, $p < 0.0001$), MSA (17.5% ± 10.8%, $p < 0.0001$), DLB (16.8% ± 10.6%, $p < 0.0001$), pPD (16.0% ± 9.2%, $p < 0.0001$)] (Fig. 4a, Table 2). No significant differences were observed among the synucleinopathy cohorts themselves. ROC analysis for distinguishing AD from CTL yielded an AUC of 1.0, with 100% sensitivity and specificity (Fig. 4b), positioning the tau-seeding assay as a perfect discriminator in this cohort.

Based on the criteria of the ROC analysis, well-count and threshold established with AD and CTL samples above, a subset of positive skin tau-seeding activity was also detected in all synucleinopathies: 41.9% for rPD, 50.0% – 51.0% for pPD, 47.6% – 52.4% for MSA and 33.3% for DLB (Fig. 4a, Table 2).

To rule out the possibility that the tau-seeding activity detected in PD skin samples was attributable to cross-seeding between αSyn and tau, we performed RT-QuIC assays using tau PFFs as seeds in the αSyn substrate. As expected, tau-PFFs elicited significantly earlier and greater seeding-activity than tau monomers (Fig. 4c). In contrast, the seeding-activities induced by αSyn-PFFs and αSyn monomers were comparable to that of tau monomers (Fig. 4c), indicating that αSyn-PFFs do not cross-seed the tau substrate.

We further characterized tau aggregates in the end-products of RT-QuIC assay of PD skin samples stratified by tau-seeding status. FTA using anti-tau antibody R4 revealed an intense band in tau-positive rPD reactions, which was minimal in tau-negative counterparts (Supplementary Fig. S4a). The FTA band intensity was significantly elevated in the positive tau-seeding group ($p < 0.0001$, Supplementary Fig. S4b) and exhibited a moderate positive correlation with endpoint ThT fluorescence (Supplementary Fig. S4c). TEM confirmed the presence of classical tau fibrils in positive-seeding reactions (Supplementary Fig. S4e), while negative samples were devoid of fibrillar material (Supplementary Fig. S4d). These data establish that skin not only harbors αSyn seeds but also serves as a reservoir for tau seeds, offering a dual-pathology diagnostic window.

Simoa-detected plasma biomarkers including p-tau217, GFAP and NfL levels in synucleinopathy patients with positive skin tau seeding

Simoa-detected plasma p-tau217, GFAP, and NfL have been established as effective diagnostic biomarkers for AD[22–25]. To determine whether positive skin tau-seeding activity in PD reflects comorbid AD-type pathology, we quantified these biomarkers using the Simoa platform in patients with synucleinopathies. AD patients were used as positive controls and they showed markedly elevated plasma p-tau217 and GFAP compared with both CTL and all synucleinopathy subgroups, regardless of skin tau-seeding status ($p < 0.0001$, Fig. 5a, c). Specifically, p-tau217 levels in AD (1.67 ± 1.04 pg/mL)

versus CTL (0.49 ± 0.22 pg/mL) yielded an AUC of 0.9333, with a sensitivity of 86.67% and specificity of 100% (Fig. 5b); GFAP levels in AD (200.06 ± 99.60 pg/mL) versus CTL (63.38 ± 23.15 pg/mL) yielded an AUC of 0.9846, with a sensitivity of 84.62% and specificity of 100% (Fig. 5d). By contrast, pairwise post-hoc comparisons revealed no statistically significant differences in either p-tau217 or GFAP between CTL and any synucleinopathy subgroup—including PD patients with positive (PD+) or negative (PD−) skin tau-seeding, as well as MSA/DLB patients stratified by seeding status (all $p > 0.05$, Fig. 5a, c). Likewise, no significant differences in plasma NfL were observed across any of the conditions examined (Fig. 5e, f). Collectively, these findings indicate that although a subset of PD patients harbor detectable tau-seeding activity in skin, this tauopathy occurs independently of plasma p-tau217 elevation and is thus distinct from the canonical AD-associated plasma biomarker profile.

Morphological characterization of αSyn aggregates from the RT-QuIC end-products across synucleinopathies

Having observed distinct morphological features of αSyn aggregates in RT-QuIC end-products seeded with autopsied skin samples from PD, DLB, and MSA using recombinant human αSyn as the substrate in our prior work[15], we next examined whether these differences persisted when employing recombinant mouse αSyn as the substrate in the current assay with biopsied skin samples. TEM analysis revealed typical fibrils in all synucleinopathy groups, but none in CTL, with clear morphological distinctions among the three disease types. Quantitatively, PD-seeded fibrils were the longest (226.43 ± 63.89 nm), followed by DLB (190.40 ± 36.62 nm) and MSA (110.35 ± 30.79 nm) (Fig. 6a–d), and these length differences were highly significant across groups ($p < 0.0001$, Fig. 6e). A similar trend was observed for fibril volume: PD exhibited the largest volume (7,930.54 ± 4,959.44 nm^3), significantly greater than MSA ($p < 0.0001$); DLB showed intermediate volumes (6,403.89 ± 3,657.66 nm^3), also significantly larger than MSA ($p < 0.01$); and MSA had the smallest volume (3,807.91 ± 2,662.54 nm^3) (Fig. 6g). In contrast, no significant differences in the width of fibrils among the three conditions were observed ($p > 0.05$) (Fig. 6f). Together, these morphological differences suggest that αSyn aggregates generated from biopsied skin samples of distinct synucleinopathies may possess strain-specific structural properties, even when amplified using a mouse αSyn substrate.

Correlation between skin αSyn-seeding activity and clinical manifestation of PD patients

To investigate whether peripheral αSyn-seeding activity correlates with the severity of the movement disorders in PD, we performed Pearson's correlation analyses comparing skin seeding activity against UPDRS Part III scores and H&Y scales in both rPD and pPD cohorts. No significant correlations were observed between αSyn-seeding activity and either clinical parameter across both cohorts (all $p > 0.05$; Supplementary Fig. S5). Notably, however, the two clinical scales themselves were moderately correlated

with each other in both groups (rPD: r = 0.6322, $p < 0.0001$; pPD: r = 0.5899, $p < 0.0001$), confirming their expected interrelationship despite the lack of association with the seeding assay readouts.

Correlation between skin tau-seeding activity and Simoa-detected plasma biomarkers in AD, PD, and MSA/DLB patients

We next examined the relationship between skin tau-seeding activity and Simoa-detected plasma biomarkers including p-tau217, GFAP, and NfL across different patient groups. Among AD patients, tau-seeding activity exhibited significant moderate positive correlations with plasma p-tau217 (r = 0.5692, $p = 0.003$) and GFAP (r = 0.6877, $p = 0.0003$), but not with NfL (r = 0.2035, $p = 0.340$; Supplementary Fig. S6a, b). Within this same AD cohort, p-tau217 correlated strongly with GFAP (r = 0.8933, $p < 0.0001$) and moderately with NfL (r = 0.4061, $p = 0.049$) (Supplementary Fig. S6a, b). In the PD cohort, tau-seeding activity did not correlate with any of the plasma biomarkers (all $p > 0.05$); however, a moderate correlation was observed between plasma p-tau217 and NfL (r = 0.4890, $p = 0.0045$) (Supplementary Fig. S6c, d). By contrast, in MSA/DLB patients, neither tau-seeding activity nor any pairwise combinations of the plasma biomarkers showed significant correlations (all $p > 0.05$) (Supplementary Fig. S6e, f).

Morphological characterization of tau fibrils generated by RT-QuIC from skin samples of AD and PD patients

To determine whether tau fibril morphology varies with the seeding source, we examined RT-QuIC end-products generated from skin biopsies of AD (n = 3) and PD (n = 3) patients that were positive for tau-seeding activity by TEM. Abundant fibrillar aggregates were observed in both groups (Supplementary Fig. S7a, b). Quantitative morphometric analysis uncovered distinct intergroup differences. Although fibril length did not differ significantly between the two groups (Supplementary Fig. S7c), AD-seeded fibrils exhibited significantly greater width (4.89 ± 1.27 nm vs. 3.97 ± 1.01 nm, $p < 0.01$) and larger volume (2,251.78 ± 1,380.23 nm^3 vs. 1,586.33 ± 1,189.06 nm^3, $p < 0.05$) than their PD-seeded counterparts (Supplementary Fig. S7d, e).

Discussion

Our current study leveraged skin-based RT-QuIC assays for both αSyn- and tau-seeding activities, combined with high sensitivity plasma biomarker measurements, to dissect the relationship between peripheral protein aggregation and systemic AD type pathology in patients with PD, MSA and DLB. Our results confirm the diagnostic utility of skin αSyn-seeding detection, replicate morphological strain differences among synucleinopathies, and, most importantly, uncover a striking dissociation: a significant proportion of PD patients exhibit positive skin tau-seeding activity despite having plasma p-tau217 and GFAP levels within the normal range, distinct from the canonical AD profile.

The current RT-QuIC assay using recombinant mouse αSyn as a substrate demonstrated an excellent diagnostic performance in both retrospective and prospective PD cohorts, with AUC values exceeding 0.96, sensitivities and specificities around 90% and 95%, respectively. These findings align with prior reports[10–15] and extend them by establishing robust cutoffs and well count criteria that are reproducible across independent cohorts. The morphological characterization of αSyn fibrils generated from patient skin samples further reinforces the concept of strain specific conformations[26,27], as PD derived-fibrils were significantly longer and larger than those from MSA and DLB, consistent with our earlier observations using human αSyn substrate[15]. Importantly, the use of mouse αSyn as substrate did not abolish these inter disease morphological differences, suggesting that the intrinsic seeding properties of the patient-derived seeds, rather than the substrate species, dictate the final fibril architecture. This supports the feasibility of using a single recombinant substrate for broad diagnostic screening while preserving strain discriminative information.

The intriguing finding of this study is the detection of tau-seeding activity in skin samples from a substantial subset of PD patients (approximately 40–50%), at levels comparable to those previously reported through neuropathological examinations in autopsied brain tissues[4,28]. However, unlike AD, where skin tau-seeding correlated positively with plasma p-tau217 and GFAP, no such correlation existed in PD. Moreover, plasma p-tau217 and GFAP in all PD subgroups, regardless of tau-seeding status, were indistinguishable from healthy controls, whereas AD patients exhibited dramatic elevations. Our finding about the increased levels of plasma p-tau217 in PD patients is consistent with the observation by the others[29], although no increase in the plasma p-tau217 of PD patients without cognitive impairment was also reported[30]. This clear dissociation indicates that the skin tau seeds in PD are not a surrogate for classical AD type neurodegeneration. Rather, they likely represent a distinct tauopathy, possibly related to the non-AD tau isoforms (e.g., 4R tau) that have been described in PD brain pathology[1,4,7,30] or even to tau conformers that do not engage the same peripheral biomarker cascade. The morphological differences we observed between tau fibrils from AD and PD skin samples, greater width and volume in AD, further support the notion of distinct tau strains, as similar structural heterogeneity has been linked to different clinical phenotypes in tauopathies. The current findings from biopsied skin samples are consistent with our previous observations from a matched autopsy study of skin and brain tissues, which showed that although tau-seeding activity was detectable in skin samples, no AD comorbidity was detected in the same PD cases[15]. Notably, tauopathies in PD were mainly observed in dopaminergic neurons of the nigrostriatal region, contrasting with the wide-spread distribution pattern of tauopathies in AD[31]. Although tau pathology has been reported in the brains of PD patients, current cryo-EM studies have not defined a tau protein fold specific to PD up to date[32,33].

The strong correlation between skin tau-seeding and both p-tau217 and GFAP in AD patients validates our assay's biological relevance and confirms the expected link between peripheral tau aggregation and systemic AD related astrogliosis (GFAP) and tau phosphorylation (p-tau217). In contrast, the complete lack of such correlations in PD and MSA/DLB suggests that the tau seeds detected in these conditions are biochemically distinct, perhaps lacking the specific phosphorylation epitopes recognized by plasma

p-tau217 assays, or arising from a different isoform (e.g., 4R tau) that does not produce the same plasma signature. The moderate correlation between p-tau217 and NfL in PD, but not in AD or MSA/DLB, may reflect differential axonal injury dynamics in PD, but this secondary observation warrants further investigation.

Our results have important clinical implications. First, they suggest that skin biopsy combined with RT-QuIC can simultaneously interrogate αSyn- and tau-seeding, offering a minimally invasive window into two major proteinopathies that frequently co-occur in aging and neurodegenerative diseases. Second, the discordance between skin tau-seeding and plasma p-tau217 in PD challenges the assumption that peripheral tau aggregation necessarily signals AD pathology. This could be clinically valuable: in a PD patient with cognitive decline, a positive skin tau-seeding test might raise suspicion for non-AD tauopathy rather than prompting an AD diagnosis, thereby guiding appropriate therapeutic and prognostic considerations. Third, the absence of correlation between skin αSyn-seeding and severity of movement disorders (UPDRS III, H&Y) reinforces the notion that seeding-activity reflects the presence of pathology rather than its functional impact, consistent with the concept that misfolded protein seeds can accumulate long before clinical symptoms become severe.

Several limitations should be acknowledged. The sample sizes for some subgroups, particularly DLB and the morphological tau analyses (n = 3 per group), are small, and the findings require replication in larger, well characterized cohorts. Neuropathological confirmation was not available, so the precise nature of the tau species detected in skin remains speculative. Additionally, the skin biopsies were taken from a single anatomical site (neck C7 paravertebral area); it has been shown that αSyn-seeding activities differ across body regions[32]. Longitudinal studies are needed to determine whether skin tau-seeding status predicts future cognitive decline or conversion to dementia, and whether it precedes or follows central tau accumulation. Indeed, tau-seeding activity has been reported for even prior to the earliest stages of AD changes, including in normal, and even young individuals, with prevalence across different neurodegenerative disorders for defining disease subtypes[33,34]. Finally, while we employed a tau RT-QuIC substrate based on a 4R tau fragment, the assay may not capture all tau isoforms[17,19, 35,36]; future work with multiple tau substrates could help characterize the specific strains present.

In summary, we have demonstrated that skin-based RT-QuIC can concurrently detect αSyn- and tau-seeding activities with high sensitivity in PD and related disorders. The unexpected finding of positive tau-seeding in a large subset of PD patients, without corresponding elevations in plasma p-tau217 or GFAP, points to the existence of a tauopathy that is distinct from AD. This divergence underscores the heterogeneity of PD and highlights the need for multimodal biomarker approaches that integrate tissue-based seeding assays with fluid-based markers to accurately stratify patients and guide personalized management. Our results open new avenues for investigating the role of non-AD tau pathology in PD progression and for developing therapeutic strategies targeting specific protein conformations.

Methods

Study subjects and skin biopsy collection

This study encompassed both biomarker development and clinical validation using skin biopsy specimens. The research protocol was approved by the Institutional Review Board of the First Affiliated Hospital of Nanchang University, and written informed consent was obtained from all participants. Skin samples were obtained from two independent cohorts. The retrospective cohort included patients with clinically probable PD (rPD, n = 43), MSA (n = 21), DLB (n = 3), AD (n = 15), and healthy controls (CTL, n = 34). A prospective cohort of clinical possible PD patients (pPD, n = 104) was enrolled separately. All diagnoses were established according to current International Parkinson and Movement Disorder Society (MDS) diagnostic criteria for PD[37], MSA[38,39], DLB[40], and AD[25]. Punch skin biopsies (3 mm) mainly containing epidermis and dermis were obtained from the neck (C7 paravertebral: 5 cm from the midline)[11], immediately frozen in PBS, and stored at − 80°C until processing.

Recombinant protein expression and pre-formed fibril (PFF) preparation

Recombinant mouse or human αSyn bearing an N-terminal methionine residue and a 6×His tag was expressed in *E.* coli and purified via nickel-affinity chromatography, followed by size-exclusion fast protein liquid chromatography (FPLC), following established protocols[15, 41,42]. The purity and identity of the proteins were confirmed by Coomassie Blue staining and western blotting with anti-αSyn antibody D37A6 for mouse αSyn and MJFR14 for human αSyn. Preformed fibrils (PFFs) were generated by incubating monomeric proteins at 37°C under continuous agitation in the presence of thioflavin T (ThT), with minor modifications to a previously described method[43], fibrillization kinetics were monitored in real time using a BMG plate reader. Far-UV circular dichroism (CD) spectroscopy was employed to confirm the conformational transition from an unstructured/α-helical state to a β-sheet-rich fibrillar state, as detailed elsewhere[44].

RT-QuIC assay for αSyn

RT-QuIC assays for detecting skin αSyn-seeding activity were performed as previously described[10,15,42], with modifications below. Briefly, skin samples were homogenized to a 10% (w/v) concentration in a lysis buffer composed of Tris-buffered saline (TBS) containing 2 mM CaCl2 and 0.25% (w/v) collagenase A (Roche, USA). The samples were incubated at 37°C for 4 hours with agitation at 350 rpm, followed by further homogenization using a Mini-BeadBeater. The homogenates were centrifuged at 2,000 g for 10 min and the supernatants were kept at -80°C for future use. The RT-QuIC reaction mixture consisted of 40 mM phosphate buffer (pH 8.0), 150 mM NaCl, 7.35% ammonium sulfate, 0.1176% Triton X-100, 0.12 mg/mL recombinant mouse αSyn, and 10 μM ThT. Aliquots of the mixture (98 μL for 96-well plate or 49 μL for 384-well plate) were dispensed into a black plate, and 2 μL or 1 μL of skin homogenate diluted to 10^{-1} and 7×10^{-2} were added to each well. The plate was sealed and incubated at 50°C in a BMG LABTECH FLUOstar Omega plate reader configured for automated fluorescence readings. The total incubation lasted for 60–100 hours as designated based on differentiation of the samples, with cycles

consisting of 1 min of double-orbital shaking (700 rpm) followed by 1 min of rest. ThT fluorescence was recorded in real time throughout the run, with measurements every 45 minutes. Positive cases were defined using three criteria: (1) receiver operating characteristic (ROC) curve analysis, yielding the area under the curve (AUC), sensitivity, and specificity; (2) a fluorescence threshold set at the mean endpoint intensity of normal controls plus a predetermined multiple of the standard deviation (SD) mainly based on the ROC analysis in the retrospective cohort; and (3) the presence of a positive signal in at least 2 out of 4 replicate wells.

Preparation of recombinant human mutant 4R tau fragment and tau RT-QuIC assay

Recombinant human cysteine-free 4R tau fragment, bearing cysteine to serine substitutions at residues 291 and 322 (C291S and C322S), was prepared for serving as the substrate and for pre-formed fibrils as seeds for tau RT-QuIC, as previously described[17,42], with minor modifications. In brief, BL21-DE3 *E*. coli cells were transformed with a plasmid encoding the 4RCF tau construct. Cultures were grown at 37°C with shaking until the OD600 reached ~ 0.6, at which point protein expression was induced with 1 mM IPTG for an additional 4 hours. Cells were harvested by centrifugation, resuspended in lysis buffer (50 mM NaH2PO4, pH 8.0, 300 mM NaCl), and sonicated at 60% amplitude for 10 min. The lysate was clarified by centrifugation, and the resulting supernatant was loaded onto a Ni-NTA column pre-equilibrated with the same lysis buffer. Recombinant protein was eluted with elution buffer (50 mM NaH2PO4, pH 8.0, 300 mM NaCl, 200 mM imidazole). The pooled fractions were concentrated to 4 mL using 10 kDa molecular weight cut-off (MWCO) spin concentrators (Millipore) and filtered through 0.22 μm low-binding Durapore PVDF membrane filters (Millipore). The 4R tau fragment was further purified by size-exclusion chromatography (FPLC) using Superdex 75 and Superdex 200 columns (GE Healthcare) equilibrated with 1 × PNE buffer (25 mM PIPES, 150 mM NaCl, 1 mM EDTA, pH 7.0). The final purity exceeded 90%, as assessed by SDS-PAGE. Protein concentrations were determined using the BCA assay (ThermoFisher Scientific, USA).

For the 4R tau RT-QuIC assay[17], the reaction mixture comprised 10 mM HEPES (pH 7.4), 240 mM NaCl, 50 μM heparin, 10 μM ThT, and 0.2 mg/mL recombinant 4R tau substrate. Skin homogenates (10%, w/v) were centrifuged at 3,000 g for 10 min at 4°C. The resulting supernatant was diluted 1:200 in a buffer containing 10 mM HEPES, 1× N2 supplement (Gibco), and 1× PBS, and then further centrifuged at 5,000 g for 5 min at 4°C. Aliquots of the reaction mixture (98 μL) were dispensed into each well of a 96-well plate, followed by seeding with 2 μL of the diluted, clarified skin supernatant. The plate was sealed and incubated at 50°C in a BMG FLUOstar Omega plate reader, where the reaction was subjected to continuous orbital shaking at 500 rpm throughout the assay. ThT fluorescence was measured and analyzed as mentioned above.

Filter-trap assay and immunoblotting

The filter trap assay (FTA) is a generally recognized, user-friendly *in vitro* method for differentiating detergent-insoluble protein aggregates from their detergent soluble monomers including misfolded αSyn

aggregates. FTA was conducted as previously described[15,20,21]. In brief, the RT-QuIC end products were diluted in washing buffer (2% SDS, 10 mM Tris-HCl, pH 8.0, and 150 mM NaCl) and incubated for 1 hour at room temperature. After incubation, the samples were filtered through a cellulose acetate membrane (Advantec MFS, Dublin, CA, USA). The membrane was then rinsed with washing buffer containing 0.1% SDS in 1× PBS and blocked with 5% BSA and 0.1% Tween 20 in 1 × PBS for 1 hour to prevent nonspecific binding. Subsequently, the membrane was probed with primary antibodies (anti-αSyn antibodies D37A6 or MJFR14, or anti-tau antibody R4), followed by incubation with an HRP-conjugated goat anti-rabbit secondary antibody. Immunoreactive signals were visualized via chemiluminescence, and band intensities were semi-quantified using ImageJ software.

Fluorescence microscopy and Congo red staining

The RT-QuIC end-products kept in the wells of 96-well plates were directly examined and recorded by fluorescence microscopy (FM); for Congo red staining (CRS), the samples were spotted onto glass slides, air-dried, and stained with Congo red as previously described[21]. Images were captured using a fluorescence microscope (magnification 20 x). Positive staining was defined by intense fluorescent or red-stained aggregates.

Transmission electron microscopy

Transmission electron microscopy (TEM) of protein fibrils was performed as previously described[15,21,44]. Briefly, a 3–5 µL aliquot of the RT-QuIC end product was deposited onto a 230-mesh carbon-coated copper grid that had been glow-discharged prior to use. After a 60 s incubation, the excess sample was blotted away with filter paper. The grid was then briefly washed with 3 µL of 2% uranyl acetate and subsequently stained with another 3 µL of the same stain for 60 s, after which the staining solution was removed by blotting. After air drying, the grid was examined under a transmission electron microscope operating at 120 kV.

Simoa detection of plasma biomarkers

The blood samples collected into tubes containing EDTA as an anticoagulant were allowed to stand at room temperature for 30 min and were then centrifuged at 3,600 rpm for 10 min at 4°C to isolate the plasma fraction. The resulting plasma supernatants were aliquoted and immediately stored at − 80°C until further analysis. Concentrations of the plasma biomarkers including phosphorylated tau 217 (p-tau217), GFAP, and NfL were detected using the ultrasensitive Simoa HD-X platform (Quanterix, Billerica, MA, USA) and ALZpath pTau217 Advantage PLUS Reagent kit (Cat. no.104570, N2PB Advantage PLUS Reagent Kit (Cat. no. 104670), following the manufacturer's instruction. To minimize technical variability, all samples were analyzed in a single, randomized, and blinded run using reagents from the same production lots. All measured concentrations fell within the standard linear dynamic ranges. Samples out of the range were excluded from subsequent analyses.

Western blotting

Western blotting of recombinant mouse and human αSyn was conducted based on the previously described[15,21]. In brief, the samples were separated using home-made 12.5% SDS-PAGE mini gels. Proteins were transferred onto Immobilon-P polyvinylidene fluoride (PVDF, Millipore) membranes from the gels for 90 min at 70V. After blocking for non-specific bindings with 5% BSA, 0.1% Tween-20 in 1 × PBS, the proteins were immunoblotted with primary monoclonal antibody D37A6 for mouse αSyn (1:1,000, Thermo Fisher, USA), or MJFR14 (1:2,000, Thermo Fisher, USA) for human αSyn, for 2 hours at room temperature. The blots were then washed with washing buffer containing 5% fat-free milk in TBS and 0.1% Tween-20 for 3 times, 10 min/time, followed by incubation with the HRP-conjugated secondary antibody goat anti-rabbit at 1:10,000 dilution for 1 hour at room temperature. The proteins were visualized using ECL Plus, and the resulting signal was captured using a Bio-Red ChemiDoc™chemiluminescent imaging system.

Statistical Analysis

Data are expressed as median and interquartile range. Comparisons between two groups were performed using Mann-Whitney U tests, and multiple-group comparisons used Kruskal-Wallis tests with Dunn's post-hoc correction. Diagnostic performance was evaluated by receiver operating characteristic (ROC) curve analysis, calculating the AUC, sensitivity, and specificity. Correlations were assessed by Spearman's rank test. A p-value < 0.05 was considered statistically significant. All statistical analyses were performed using GraphPad Prism.

Declarations

Acknowledgments

We gratefully acknowledge all the participants who donated skin samples for this study, as well as the physicians and nurses of the First Affiliated Hospital of Nanchang University for their invaluable assistance in collecting clinical data and samples.

Availability of data and materials

The raw data that supports the findings of this study are available from the corresponding author upon request.

Funding

This work was partially supported by the startup package and developmental funds of the First Affiliated Hospital of Nanchang University (500021001, 500021002), National Natural Science Foundation (NSFC) (82471499) to WQZ, and Jiangxi Key Laboratory of Neurological Diseases (2024SSY06072) to DH and WQZ.

Author contributions

WQZ contributed to the conception and design of the work. YC performed all αsyn-related experiments. YW conducted tau-related experiments. KN and YW did Simoa-related experiments. ZJ participated FTA/WB experiments and partial RT-QuIC assay. HY participated in initial αSyn RT-QuIC work. ZW, HM, YK, HY, SL, PYX, AF, VD, YS, XH, and ZW participated in data analyses. YC, YW, ZJ, HY, ZZ, JH, YS, XC, SH, CW, JZ, XF, and DH participated in setting up the cohorts and collecting skin samples. All authors were responsible for the acquisition, analysis and interpretation of data. YC and WQZ wrote the first version of the manuscript. Critical revision of the manuscript for important intellectual content was performed by all authors. All authors agreed with the content of the article to be submitted. All authors reviewed and approved the final manuscript.

Ethics approval and consent to participate

The entire approval for this study was obtained from the ethic committee of the First Affiliated Hospital of Nanchang University (Approval No. IIT 2023 Clinical Ethics Review No. 145-2). Following the Declaration of Helsinki, written informed consent was obtained from all participants or their guardians.

Consent for publication

Not applicable.

Competing interests

The author(s) declared no potential conflicts of interest with respect to the research, authorship, and/or publication of this article.

References

1. Irwin, D.J. et al. Neuropathologic substrates of Parkinson disease dementia. *Ann. Neurol.* 72, 587–598 (2012).
2. Nguyen, P.H. & Derreumaux P. Status of Alzheimer's and Parkinson's Disease Detections and Treatments. *ACS Chem. Neurosci.* 17, 2441–2453 (2026).
3. Coakeley, S. & Strafella, A.P. Imaging tau pathology in Parkinsonisms. NPJ *Parkinson's Dis.* 3, 22 (2017).
4. Zhang, X. et al. Tau pathology in Parkinson's disease. *Front. Neurol.* 9, 809 (2018).
5. Tropea, T.F. et al. Association between Plasma P-tau217 and Alzheimer's Copathology and Cognitive Decline in Parkinson's Disease. *Ann. Neurol.* 99, 1428–1437 (2026).
6. Compta, Y. et al. Lewy- and Alzheimer-type pathologies in Parkinson's disease dementia: which is more important? *Brain* 134, 1493–1505 (2011).
7. Dickson, D.W. Parkinson's disease and parkinsonism: neuropathology in Cold Spring Harbor perspectives in medicine [ed. Dickson, D.W.] 1–17 (Cold Spring Harbor Laboratory Press, 2012).

8. Palmqvist, S. et al. Discriminative Accuracy of Plasma Phospho-tau217 for Alzheimer Disease vs Other Neurodegenerative Disorders. *JAMA* 324, 772–781 (2020).
9. Thijssen, E.H. et al. Plasma phosphorylated tau 217 and phosphorylated tau 181 as biomarkers in Alzheimer's disease and frontotemporal lobar degeneration: a retrospective diagnostic performance study. *Lancet Neurol.* 20, 739–752 (2021).
10. Wang, Z. et al. Skin alpha-Synuclein Aggregation Seeding Activity as a Novel Biomarker for Parkinson Disease. *JAMA Neurol.* 78, 1–11 (2020).
11. Donadio, V. et al. In Vivo Diagnosis of Synucleinopathies: A Comparative Study of Skin Biopsy and RT-QuIC. *Neurology.* 96, e2513-e2524 (2021).
12. Manne, S. et al. Blinded RT-QuIC Analysis of alpha-Synuclein Biomarker in Skin Tissue From Parkinson's Disease Patients. *Mov. Disord.* 35, 2230–2239 (2020).
13. Mammana, A. et al. RT-QuIC Detection of Pathological alpha-Synuclein in Skin Punches of Patients with Lewy Body Disease. *Mov. Disord.* 36, 2173–2177 (2021).
14. Bsoul, R. et al. Accurate detection of pathologic alpha-synuclein in CSF, skin, olfactory mucosa, and urine with a uniform seeding amplification assay. *Acta Neuropathol. Commun.* 13, 113 (2025).
15. Gerasimenko, M. et al. Biochemical signatures of skin alpha-synuclein in synucleinopathies revealed by RT-QuIC assay end-product analysis. *Acta Neuropathol.* 151, 3 (2026).
16. Höglinger, G.U. et al. A biological classification of Parkinson's disease: the SynNeurGe research diagnostic criteria. *Lancet Neurol.* 23, 191–204 (2024).
17. Wang, Z. et al. Seeding activity of skin misfolded tau as a biomarker for tauopathies. *Mol. Neurodegener.* 19, 92 (2024).
18. Dellarole, I.L. et al. Tau seeding activity in skin biopsy differentiates tauopathies from synucleinopathies. *npj Parkinsons Dis.* 10, 116 (2024).
19. Martinez-Valbuena, I., Tartaglia, M.C., Fox, S.H., Lang, A.E. & Kovacs, G.G. Four-Repeat Tau Seeding in the Skin of Patients With Progressive Supranuclear Palsy. *JAMA Neurol.* 81, 1228–1230 (2024).
20. Eenjes, E., Yang-Klingler, Y.J., & Yamamoto, A. Monitoring Aggregate Clearance and Formation in Cell-Based Assays in *Protein Misfolding Diseases: Methods and Protocols, Methods in Molecular Biology* (ed. Gomes, CM) 157–169 (Springer Science+Business Media 2019).
21. Yang, Y. et al. Regional variations in seeding activity, phosphorylation, and protein levels of tau in Alzheimer's disease brain. *npj Biosensing.* 2 (2025).
22. Triana-Baltzer, G. et al. Development and validation of a high-sensitivity assay for measuring p217 + tau in plasma. *Alzheimers Dement. (Amst)*. 13, e12204 (2021).
23. Cicognola, C. et al. Plasma glial fibrillary acidic protein detects Alzheimer pathology and predicts future conversion to Alzheimer dementia in patients with mild cognitive impairment. *Alzheimers Res. Ther.* 13, 68 (2021).
24. Zhou, W. et al. Plasma neurofilament light chain levels in Alzheimer's disease. *Neurosci. Lett.* 650, 60–64 (2017).

25. Jack, C.R. et al. Revised criteria for the diagnosis and staging of Alzheimer's disease. *Nat. Med.* 30, 2121–2124 (2024).
26. Peelaerts, W. et al. alpha-Synuclein strains cause distinct synucleinopathies after local and systemic administration. *Nature* 522, 340–344 (2015).
27. Shahnawaz, M. et al. Discriminating alpha-synuclein strains in Parkinson's disease and multiple system atrophy. *Nature* 578, 273–277 (2020).
28. Lei, P. et al. Tau deficiency induces parkinsonism with dementia by impairing APP-mediated iron export. *Nat. Med.* 18, 291–295 (2012).
29. Kouchache, T. et al. Association Between Plasma Phosphorylated Tau-217 and Cognition in Parkinson's Disease. *Mov. Disord.* doi: 10.1002/mds.70400 (2026).
30. Fiorenzato, E. et al. Plasma p-tau217 Versus p-tau181 in Parkinson's Disease: Differential Associations with Alzheimer's Disease-Related Neurostructural Changes and Cognitive Function. *Mov Disord.* doi: 10.1002/mds.70392 (2026).
31. Wills, J. et al. Elevated tauopathy and alpha-synuclein pathology in postmortem Parkinson's disease brains with and without dementia. *Exp. Neurol.* 225, 210–218 (2010).
32. Scheres, S.H.W., Ryskeldi-Falcon, B. & Goedert, M. Molecular pathology of neurodegenerative diseases by cryo-EM of amyloids. *Nature* 621, 701–710 (2023).
33. Creekmore, B.C., Chang, Y.W. & Lee, E.B. The Cryo-EM Effect: Structural Biology of Neurodegenerative Disease Aggregates. *J. Neuropathol. Exp. Neurol.* 80, 514–529 (2021).
34. Liu, M. et al. Distinct cutaneous α-synuclein signatures in body-first and brain-first Parkinson's disease subtypes. *Brain* 149, 1554–1567 (2026).
35. Manca, M. et al. Tau seeds occur before earliest Alzheimer's changes and are prevalent across neurodegenerative diseases. *Acta Neuropathol.* 146, 31–50 (2023).
36. Browne, D.F. et al. Early Alzheimer's Disease with frequent neuritic plaques harbors neocortical tau seeds distinct from primary age-related tauopathy. *Nat. Commun.* 16, 1851 (2025).
37. Postuma, R.B. et al. MDS clinical diagnostic criteria for Parkinson's disease. *Mov. Disord.* 30, 1591–1601 (2015).
38. Gilman, S. et al. Second consensus statement on the diagnosis of multiple system atrophy. *Neurology* 71, 670–676 (2008).
39. Wenning, G.K. et al. The Movement Disorder Society Criteria for the Diagnosis of Multiple System Atrophy. *Mov. Disord.* 37, 1131–1148 (2022).
40. McKeith, I.G. et al. Diagnosis and management of dementia with Lewy bodies: Fourth consensus report of the DLB Consortium. *Neurology* 89, 88–100 (2017).
41. Janarthanam, C. et al. High-Yield alpha-Synuclein Purification and Ionic Strength Modification Pivotal to Seed Amplification Assay Performance and Reproducibility. *Int. J. Mol. Sci.* 25 (2024).
42. Mao, H. et al. Ultrasensitive detection of aggregated alpha-synuclein using quiescent seed amplification assay for the diagnosis of Parkinson's disease. *Transl. Neurodegener.* 13, 35 (2024).

43. Okuzumi, A. et al. Propagative alpha-synuclein seeds as serum biomarkers for synucleinopathies. *Nat. Med.* 29, 1448–1455 (2023).
44. Zou, W.Q., Yang, D.S., Fraser, P.E., Cashman, N.R. & Chakrabartty, A. All or none fibrillogenesis of a prion peptide. *Eur. J. Biochem.* 268, 4885–4891 (2001).

Tables

Tables are available in the Supplementary Files section.

Figures

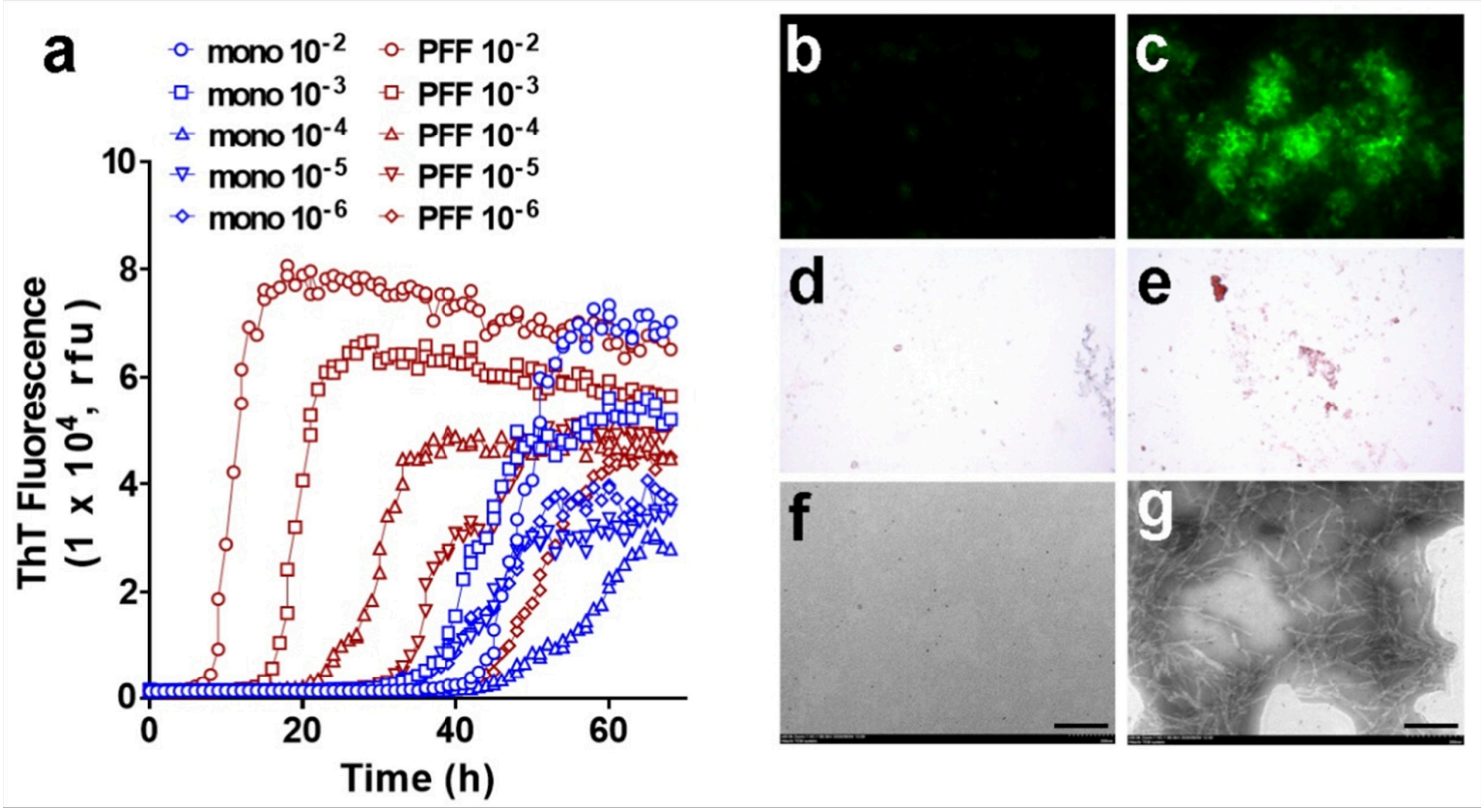


Figure 1

RT-QuIC titration of recombinant human αSyn preformed fibrils (PFFs) and characterization of *de novo* generated aggregates in end-products.

a Seeding activities of serially diluted αSyn-PFFs (10^{-2} to 10^{-6}) were assessed via RT-QuIC. Equivalent dilutions of αSyn monomer served as negative controls. While monomer-seeded reactions remained largely inactive until 35 hours, PFF-seeded samples exhibited a robust increase in ThT fluorescence starting at 10 hours of incubation. The maximal dilution permitting unambiguous discrimination between PFFs and monomer was 10^{-5}, corresponding to 0.14 fg/mL. **b-g** End-point products from PFF-seeded (**c**, **e**, **g**) and monomer-seeded (**b**, **d**, **f**) reactions were analyzed by FM (**b**, **c**), CRS (**d**, **e**), and TEM (**f**, **g**). FM

revealed bright fluorescent aggregates exclusively in PFF-seeded samples, while CRS yielded positive red staining only in these reactions. TEM further confirmed the presence of abundant amyloid fibrils in PFF-seeded end-products, contrasting with the complete absence of fibrillar structures in monomer-seeded controls. Magnifications for FM and CRS panels: 20 x; TEM scale bars: 200 nm.

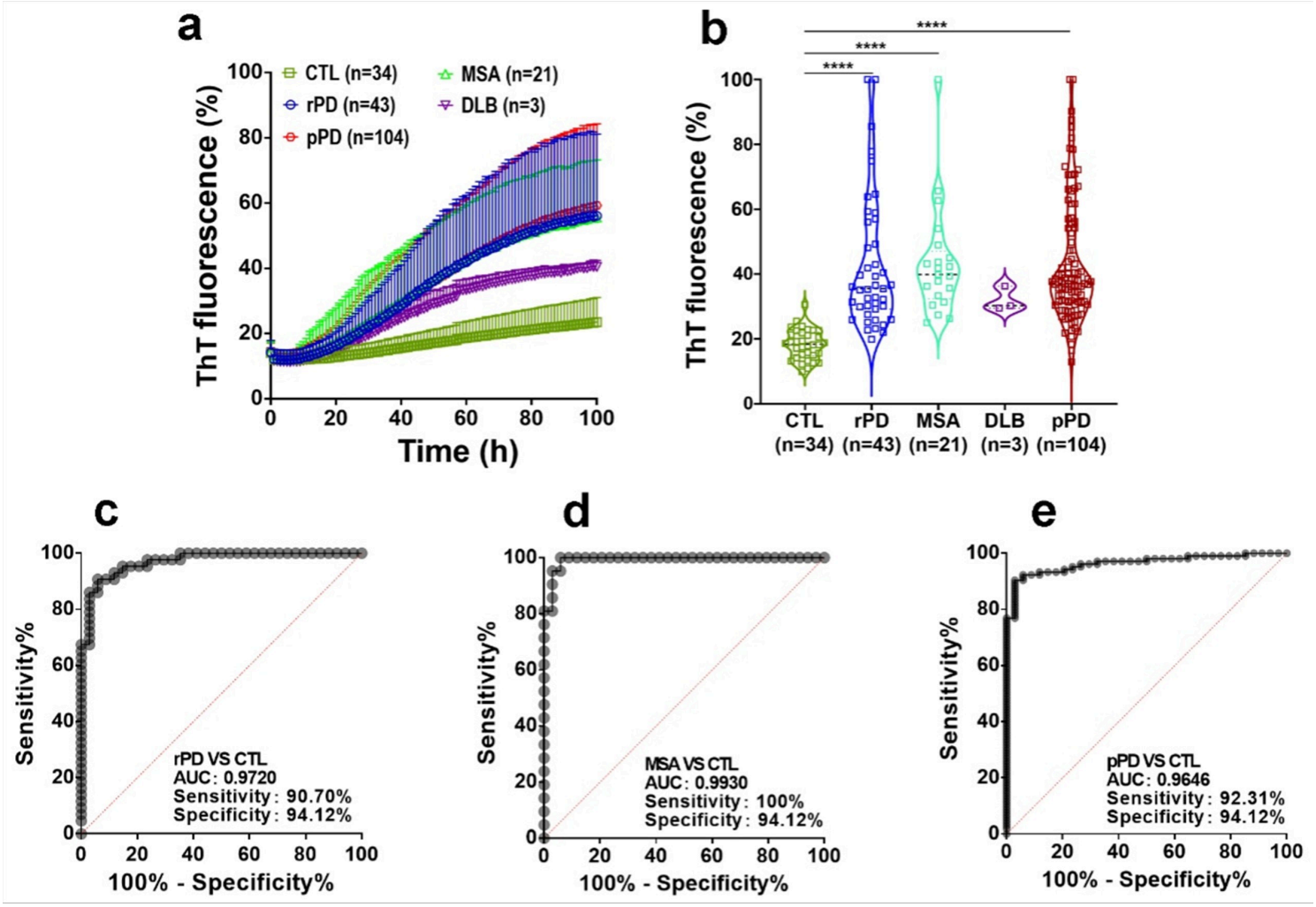


Figure 2

Detection of αSyn seeding activity in human skin samples via RT-QuIC.

Skin specimens obtained from two independent cohorts including a retrospective cohort comprising patients with rPD (n = 43), MSA (n = 21), DLB (n = 3), and CTL (n = 34), as well as a prospective cohort of PD patients (pPD, n = 104) were examined by RT-QuIC for αSyn-seeding activity. **a**Real-time kinetic curves showing the percentage of ThT fluorescence over time for skin samples from each diagnostic group. **b** Scatter dot plots (with median and interquartile range) depicting the endpoint ThT fluorescence intensities (%) for individual samples across all groups. **c**-**e**Receiver operating characteristic (ROC) curves evaluating the diagnostic accuracy of the skin RT-QuIC assay for discriminating rPD versus CTL (**c**), MSA versus CTL (**d**), and pPD versus CTL (**e**).

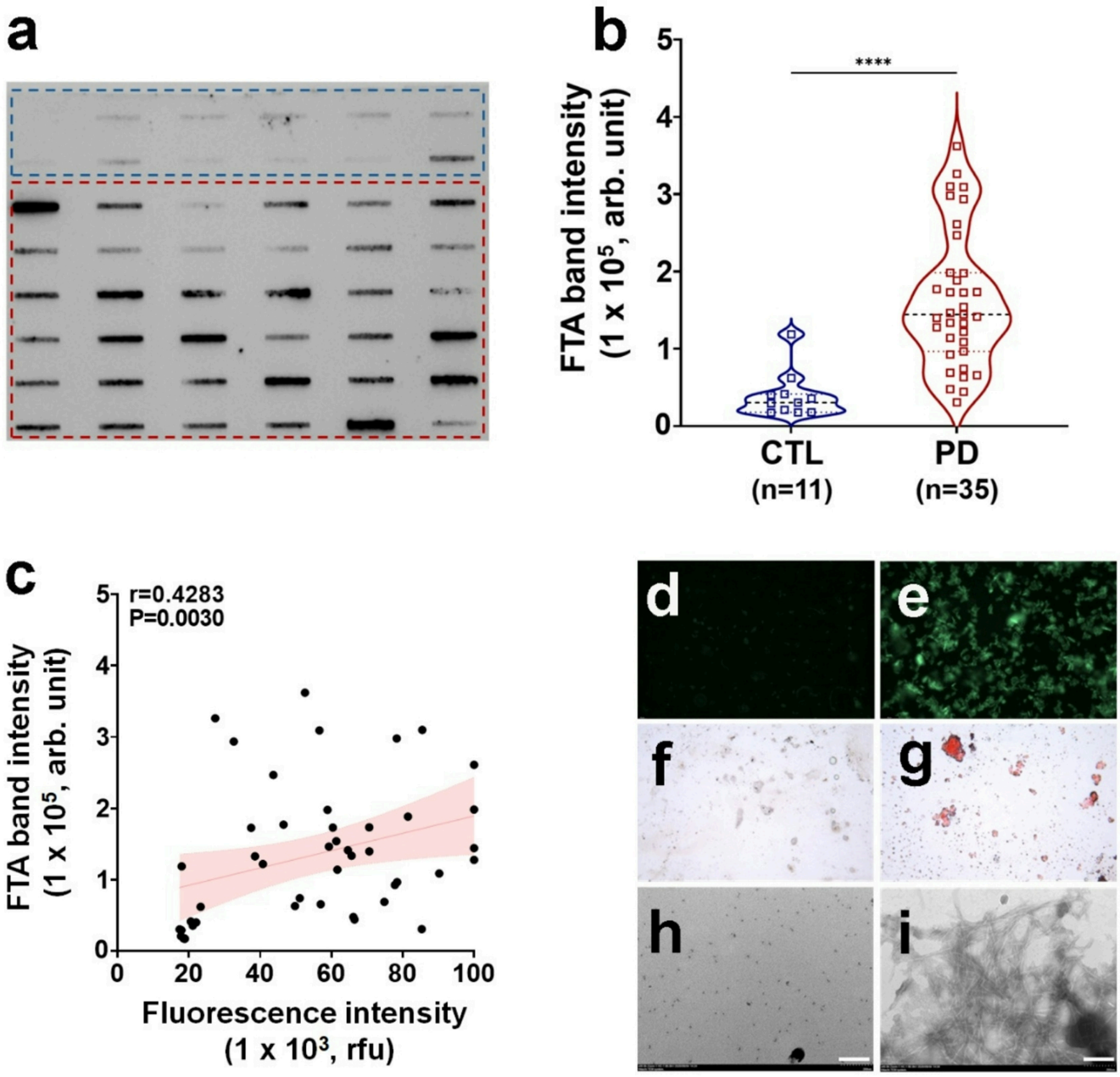


Figure 3

Characterization of αSyn aggregates in RT-QuIC reaction end-products derived from skin samples of the rPD cohort.

Endpoint reaction products of RT-QuIC from the skin of rPD patients and CTL subjects were analyzed using filter-trap assay (FTA), FM, CRS, and TEM. **a** FTA immunoblot probed with the anti-αSyn antibody D37A6. Lanes loaded with αSyn-PFF and αSyn-monomer are shown on the upper left of each dashed box as the positive and negative assay controls, respectively. rPD-seeded reaction products (red dashed box)

exhibited a marked αSyn band intensity, whereas CTL-seeded products (blue dashed box) displayed only minimal signal. **b** Violin scatter plots quantifying FTA band intensities for CTL (n = 11) and rPD (n = 35) end-products. Band intensity was significantly higher in the rPD group compared to the CTL group ($p < 0.0001$). **c** Correlation between FTA band intensity and ThT fluorescence intensity across all samples. A weak-to-moderate positive correlation was observed (Spearman's $\rho = 0.4283$, $p = 0.002$). FM of CTL samples showed negligible background staining **(d)**, whereas rPD samples exhibited intense fluorescent αSyn aggregates **(e)**. CRS showed no positive red-stained amyloid structures in CTL controls **(f)** but clearly present in rPD end-products **(g)**. TEM revealed abundant, typical amyloid fibrils in rPD-seeded reactions **(i)**, whereas no fibrillar or filamentous material was detectable in CTL-seeded samples **(h)**. Magnification for fluorescence and CRS panels **(d–g)**: 20 x; Scale bars in TEM images **(h, i)**: 200 nm.

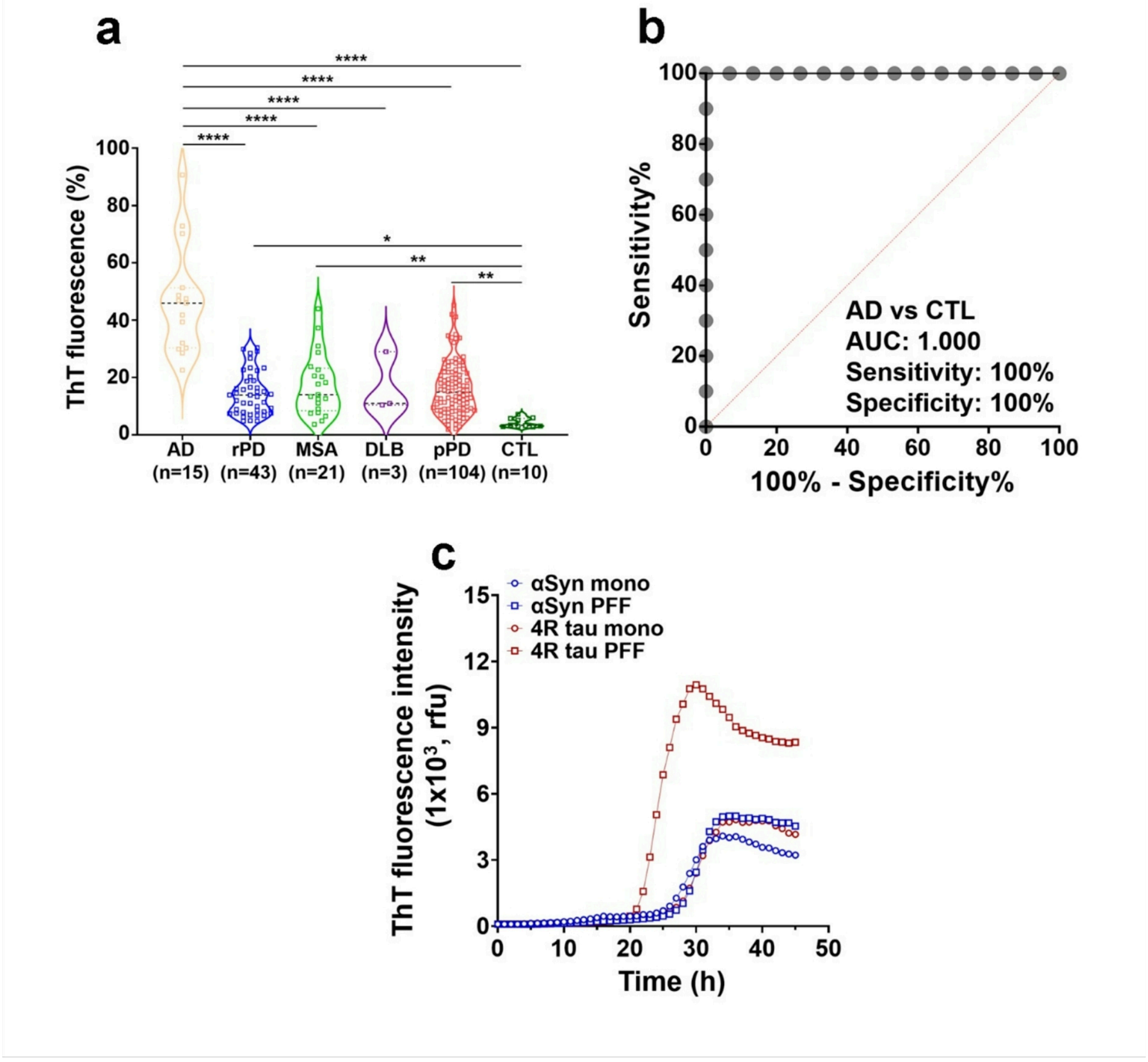


Figure 4

Detection of tau-seeding activity in skin samples by RT-QuIC assay.

a Endpoint ThT fluorescence intensities (%) measured in skin biopsies from CTL (n = 10) and patients with AD (n = 15), rPD (n = 43), MSA (n = 21), DLB (n = 3), and pPD (n = 104). AD samples showed significantly higher tau-seeding activity compared with CTL and all synucleinopathy groups (rPD, MSA, DLB, and pPD). Among the synucleinopathies, both MSA and pPD exhibited markedly elevated tau-seeding activity relative to CTL, whereas rPD and DLB did not differ significantly from CTL. No significant

differences in tau-seeding activity were observed among the synucleinopathy cohorts themselves. **b** ROC curve analysis for distinguishing AD from CTL based on skin tau-seeding activity. The AUC was 1.0, with both sensitivity and specificity reaching 100%, indicating that this assay is a highly reliable biomarker for differentiating AD from healthy, MSA, DLB and most of PD controls. **c** Real-time kinetic curves of RT-QuIC assay of recombinant tau-monomers/PFFs and αSyn-monomers/PFFs in the presence of recombinant tau as the substrate. The ThT fluorescence intensity of tau-PFF seeds was significantly higher than that of tau-monomers and αSyn-monomers/PFF seeds.

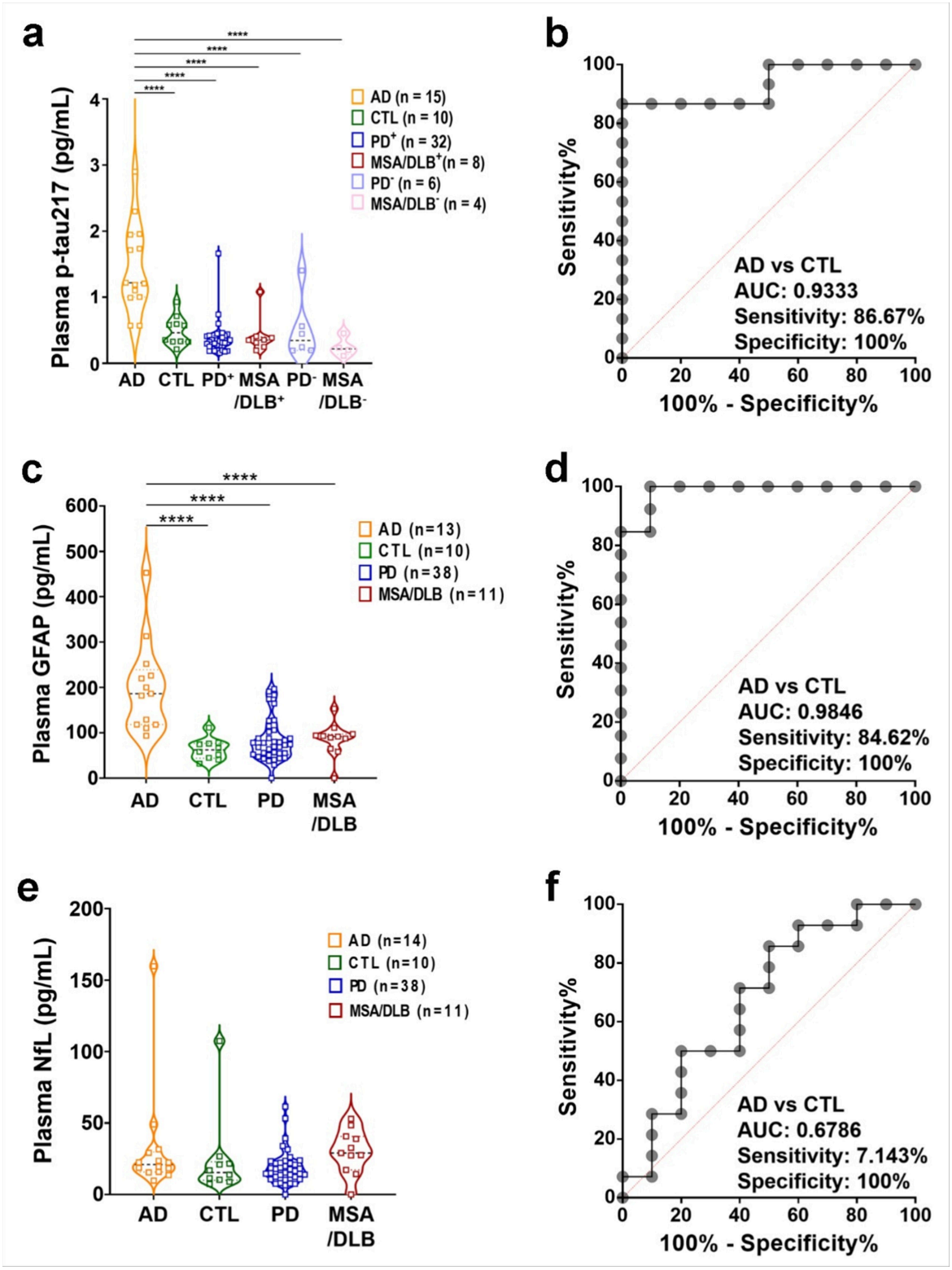


Figure 5

Quantification of plasma p-tau217, GFAP, and NfL levels using the single-molecule array (Simoa). **a, c, e** Scatter plots showing individual biomarker concentrations (pg/mL) across diagnostic groups; In panel **(a)**, PD and MSA/DLB groups are further stratified based on skin tau-seeding status (positive, +; negative, −), whereas in panels **(c)** and **(e)** these groups are shown as pooled cohorts. Sample sizes for each group are indicated in parentheses. **b, d, f** ROC curves evaluating the diagnostic performance of each biomarker in distinguishing AD patients from non-AD CTL individuals. *p < 0.05, **p < 0.01, ***p < 0.001, ****p < 0.0001.

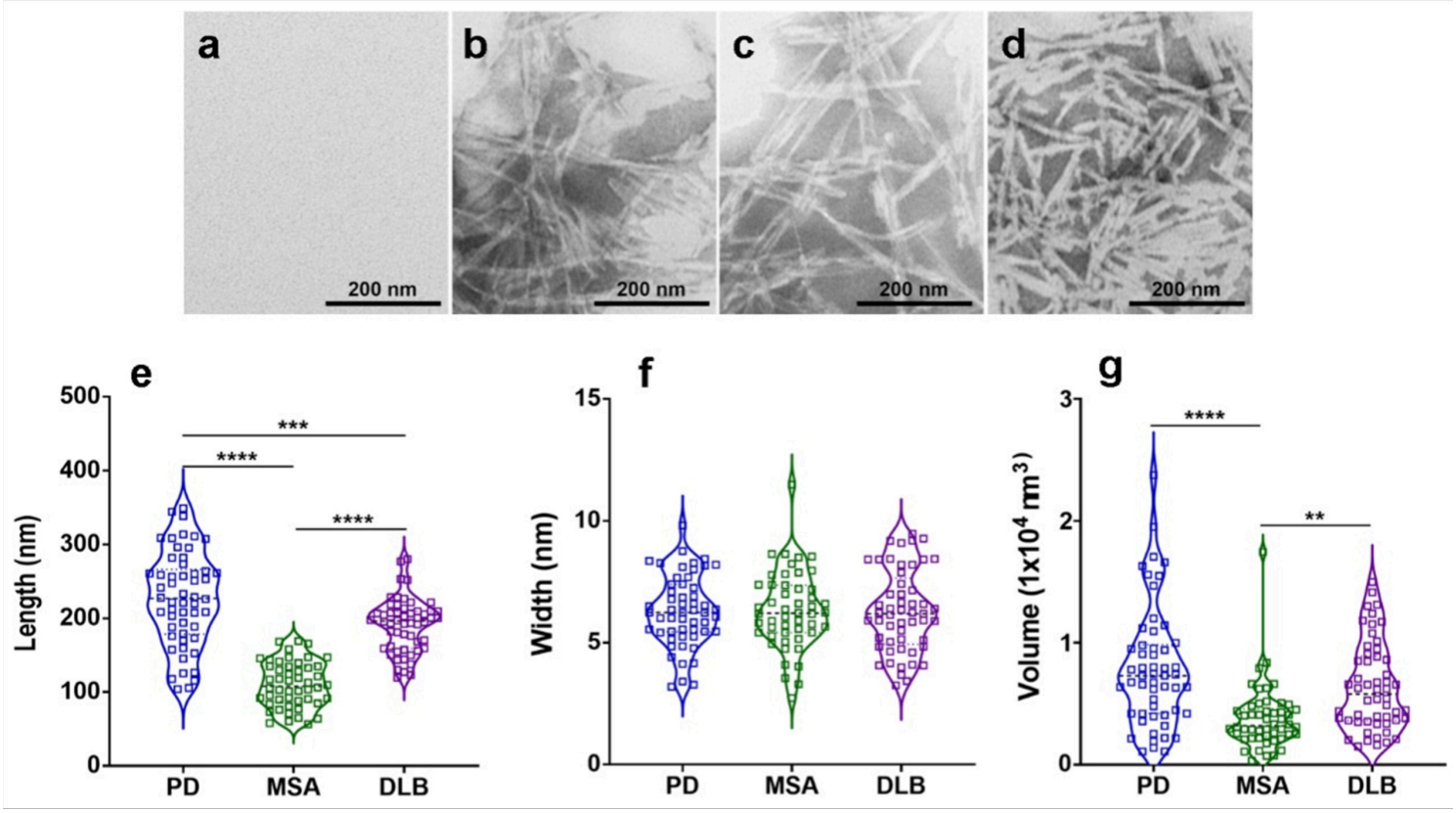


Figure 6

Morphological characterization of αSyn aggregates generated by RT-QuIC from skin samples of patients with different synucleinopathies.

End-products from skin-seeded RT-QuIC reactions derived from CTL (n = 3), PD (n = 3), DLB (n = 3), and MSA (n = 3) patients were analyzed by TEM. Representative images are shown in panels **a**–**d**. No fibrillar structures were observed in CTL-derived end-products (panel **a**), whereas abundant fibrillar aggregates were readily detected in all three synucleinopathy groups (panels **b**–**d**). Quantitative image analysis revealed that PD-seeded fibrils were significantly longer than DLB-seeded fibrils, which in turn were significantly longer than MSA-seeded fibrils (both ****p< 0.0001) (**e**). For fibril volume, PD and DLB aggregates both exhibited greater volume than MSA samples-deeded aggregates (PD vs. MSA: ****p< 0.0001; DLB vs. MSA: **p < 0.01), whereas no significant difference was found between PD and DLB (p >

0.05) (**g**). No significant differences in fibril width were observed among the three groups ($p > 0.05$) (**f**). Each dot represents an individual fibril measured from each condition. Scale bars: 200 nm.

Supplementary Files

This is a list of supplementary files associated with this preprint. Click to download.

- Supplementaryfigures.docx
- Tables.docx